Research Square

Preprints are preliminary reports that have not undergone peer review.
They should not be considered conclusive, used to inform clinical practice,
or referenced by the media as validated information.

Clozapine and Metabolic Syndrome: Evidence from Integrative Bioinformatics and Molecular Simulation

Chuanjun Zhuo

zhuochuanjun@tmu.edu.cn

Tianjin Anding Hospital, Nankai University Affiliated Tianjin Anding Hospital, Tianjin Mental Health Center of Tianjin Medical University https://orcid.org/0000-0002-3793-550X

Ximing Chen

Tianjin Anding Hospital https://orcid.org/0009-0000-8349-1551

Ranli Li

Xiaoyan Ma

Hongjun Tian

Tianjin Fourth Center Hospital https://orcid.org/0009-0006-2438-6798

Article

Keywords: clozapine, metabolic syndrome, network pharmacology, bioinformatics, molecular docking, molecular dynamic simulation

Posted Date: November 2nd, 2026

DOI: https://doi.org/10.21203/rs.3.rs-11327477/v1

License: This work is licensed under a Creative Commons Attribution 4.0 International License. Read Full License

Additional Declarations: The authors have declared there is **NO** conflict of interest to disclose

Abstract

Clozapine is an effective treatment for treatment-resistant schizophrenia, but its clinical use is limited by the high risk of developing metabolic syndrome (MetS). This study aimed to identify potential molecular targets and biological mechanisms underlying clozapine-induced MetS. We integrated clozapine-related targets, MetS-related genes, and differentially expressed genes from the GSE98895 dataset to identify candidate targets. We used functional enrichment analysis and machine learning algorithms, including least absolute shrinkage and selection operator, random forest, support vector machine recursive feature elimination, and extreme gradient boosting, to identify hub genes. We then performed gene set enrichment analysis, gene set variation analysis, and immune cell composition analysis to characterize the biological and immunological features associated with these genes. Subsequently, we used molecular docking, molecular dynamics simulations, and molecular mechanics/Poisson–Boltzmann surface area analysis to evaluate potential interactions between clozapine and the identified proteins. Thirteen overlapping targets were identified and were primarily enriched in pathways related to T helper (Th) 1 and Th2 cell differentiation, Th17 cell differentiation, and necroptosis. Janus kinase 1 (*JAK1*) and poly (ADP-ribose) polymerase 1 (*PARP1*) were consistently selected by all machine learning algorithms. *JAK1* expression was decreased, whereas *PARP1* expression was increased, in individuals with MetS, and the combined model achieved an area under the receiver operating characteristic curve of 0.895. Pathway analyses implicated alterations in immune signaling, mitochondrial energy metabolism, carbohydrate metabolism, circadian regulation, and cellular homeostasis. The MetS group also showed altered proportions of CD8 + T cells, resting natural killer cells, and resting memory CD4 + T cells. Structural analyses suggested that clozapine formed energetically favorable interactions and conformationally stable complexes with JAK1 and PARP1. Collectively, these findings identify *JAK1* and *PARP1* as candidate genes potentially involved in clozapine-induced MetS and provide testable hypotheses regarding the associated metabolic and immune mechanisms.

1. Introduction

Second-generation antipsychotics (SGAs) are a mainstay of schizophrenia treatment and have substantially improved the quality of life of millions of individuals worldwide[1]. Schizophrenia affects approximately 27 million people worldwide, accounting for about 0.29% of the global population[2]. Individuals with schizophrenia have a life expectancy approximately 20 years shorter than that of the general population, with cardiovascular disease (CVD) representing a major cause of premature mortality[3]. Despite their central role in the management of schizophrenia, antipsychotic medications are associated with substantial weight gain, metabolic dysregulation, and an increased risk of diabetes, all of which may further increase cardiovascular risk[4]. Accumulating evidence thus suggests that the cardiometabolic adverse effects associated with SGAs contribute substantially to the excess cardiovascular burden observed in individuals with schizophrenia [5].

Metabolic syndrome (MetS) comprises a cluster of interrelated metabolic abnormalities associated with an increased risk of CVD[6]. According to the Joint Interim Statement (JIS) criteria, MetS is diagnosed when at least three of the following five components are present: central obesity, elevated triglyceride levels, reduced high-density lipoprotein cholesterol levels, elevated blood pressure, and elevated fasting plasma glucose[7]. Individuals with schizophrenia have more than twice the risk of developing MetS compared with the general population[8]. The increased prevalence of MetS among individuals with schizophrenia has been attributed to several factors, including atypical antipsychotic use, genetic susceptibility, biological alterations associated with schizophrenia, and unhealthy lifestyle behaviors[9].

Among SGAs, clozapine and olanzapine are associated with the greatest metabolic risk, even after relatively short treatment periods[10,11]. However, discontinuing or switching antipsychotic medications is often clinically challenging, particularly in individuals receiving clozapine, because transitioning to an alternative treatment may exacerbate psychotic symptoms[12]. The molecular and cellular mechanisms through which SGAs contribute to MetS are complex and involve multiple organs and metabolic pathways. Proposed mechanisms include alterations in glucagon and insulin secretion, hepatic glucose production, lipid metabolism, fat deposition in the liver and adipose tissue, and insulin sensitivity[13].

Current management strategies, including psychoeducation, physical exercise, dietary interventions, and pharmacological treatment, may provide limited or variable benefits. Furthermore, genetic research on SGA-associated MetS remains limited. Identifying key genes and molecular pathways may facilitate targeted interventions and improve early prediction of MetS risk. A previous meta-analysis identified several potential susceptibility genes associated with clozapine-induced weight gain, including *DRD2*, *HTR2A*, *HTR2C*, *HTR3A*, and *TNF*[14]. However, existing research has focused primarily on genetic variation, with comparatively less attention given to downstream gene expression and its potential role in clozapine-induced MetS.

Accordingly, this study integrated bioinformatics and network pharmacology approaches to investigate the potential molecular mechanisms underlying clozapine-induced MetS. MetS-associated transcriptomic data were integrated with predicted clozapine targets to identify candidate molecular links for further analysis. We used multiple machine learning algorithms to identify candidate hub targets. We then performed gene set enrichment analysis (GSEA) and gene set variation analysis (GSVA) to further characterize the relevant regulatory and pathological mechanisms. Finally, we conducted molecular docking and molecular dynamics simulations to assess potential interactions between clozapine and the identified hub targets. The overall study workflow is shown in Fig. 1.

2. Materials and methods

2.1. Screening of Clozapine-Related Targets

The chemical structure and simplified molecular-input line-entry system (SMILES) string of clozapine were retrieved from the PubChem database[15]. The SMILES string was submitted to the Similarity Ensemble Approach (SEA)[16], Super-PRED[17], and TargetNet[18] databases to predict potential clozapine-related targets. In addition, the chemical structure of clozapine was submitted to the SwissTargetPrediction[19] and PharmMapper[20] databases for additional target prediction. All searches were restricted to *Homo sapiens*. The predicted targets obtained from the five databases were subsequently combined, duplicate entries were removed, and the corresponding gene names were standardized using the UniProt database[21].

2.2. Identification of Metabolic Syndrome-Related Targets

Genes associated with MetS were retrieved from the GeneCards[22] and Online Mendelian Inheritance in Man (OMIM)[23] databases. To reduce the contribution of weakly associated entries while retaining a sufficiently broad disease-gene set, genes with relevance scores above the median value (4.77) were retained. The genes obtained from GeneCards and OMIM were then combined, and duplicate entries were removed.

2.3. Identification of Clozapine–MetS Overlapping Targets

Clozapine-related targets and MetS-related genes were intersected to identify genes shared between the two datasets. The overlapping genes were visualized using the Venny platform.

2.4. Functional Enrichment Analysis

Gene Ontology (GO) and Kyoto Encyclopedia of Genes and Genomes (KEGG) pathway enrichment analyses were performed using the Database for Annotation, Visualization and Integrated Discovery (DAVID)[24]. GO enrichment analysis included three categories: biological process (BP), cellular component (CC), and molecular function (MF). The species was restricted to *Homo sapiens*. Enrichment terms with a false discovery rate (FDR) < 0.05 were considered significant.

2.5. Transcriptomic Data Processing and Analysis

To further refine gene screening, a MetS-related gene expression dataset was obtained from the Gene Expression Omnibus (GEO) database[25]. We downloaded the GSE98895 microarray dataset, generated using the GPL6947 platform (Illumina HumanHT-12 v3.0 Expression BeadChip), from GEO. The dataset comprised peripheral blood mononuclear cell samples from 20 individuals with MetS and 20 healthy controls[26]. The processed series matrix provided by GEO was used. According to the GEO record, the deposited expression data had undergone quantile normalization using Illumina GenomeStudio without background subtraction. Therefore, no additional log2 transformation or between-array normalization was applied. Probe identifiers were mapped to Entrez Gene IDs using the GPL6947 annotation. Probes without valid annotations were removed, and expression values were averaged when multiple probes mapped to the same Entrez Gene ID.

Differential expression analysis was performed using the limma package in R 4.4.1[27]. A linear model was fitted with group status as the explanatory variable and the control group as the reference, followed by empirical Bayes moderation. P values were adjusted using the Benjamini–Hochberg method. Genes with an adjusted p value < 0.05 and an absolute log2 fold change (|log2FC|) ≥ 0.5 were considered differentially expressed genes (DEGs) associated with MetS.

2.6. Identification of Candidate Genes

The clozapine–MetS overlapping genes were intersected with the DEGs identified in GSE98895 to obtain candidate genes for subsequent machine-learning analysis. The overlap was visualized using the Venny platform.

2.7. Identification of Hub Genes Using Machine Learning

Four machine learning algorithms were used to identify candidate hub genes: least absolute shrinkage and selection operator (LASSO) regression, random forest (RF), support vector machine recursive feature elimination (SVM-RFE), and extreme gradient boosting (XGBoost).

LASSO regression was performed using the glmnet package[28], with 10-fold cross-validation used to select the optimal regularization parameter. The RF model was constructed using the randomForest package[29], with 1,000 trees grown to ensure model stability and robustness. And candidate genes were ranked according to MeanDecreaseGini. SVM-RFE was implemented using the e1071 package[30], with 10-fold cross-validation folds generated using the caret package[31]. XGBoost analysis was conducted using the xgboost package[32]. For XGBoost, stratified 10-fold cross-validation was used to determine the optimal number of boosting iterations, with log-loss as the evaluation metric and early stopping after 20 rounds without improvement. The final XGBoost model was fitted using the selected number of iterations, and genes were ranked according to Gain. Genes

consistently identified by all four machine learning algorithms were defined as hub genes for subsequent analyses.

2.8. Gene Set Enrichment Analysis and Gene Set Variation Analysis

We performed GSEA[33] to investigate the potential molecular mechanisms associated with the hub genes in MetS. For each hub gene, samples were divided into high- and low-expression groups according to the median expression level. Differential expression between the two groups was assessed for all genes using limma, and genes were ranked in descending order according to the moderated t statistic for the high-versus-low contrast. The complete ranked gene list was used for GSEA, without prior DEG filtering. GO biological process and KEGG gene sets were obtained from MSigDB[34]. GSEA was performed using the clusterProfiler package[35], with gene set sizes restricted to 10–500 genes. Enrichment results with $p < 0.05$ and FDR < 0.25 were considered significant.

GSVA[36] was performed using the complete normalized expression matrix without prior DEG filtering. Hallmark gene sets from MSigDB were used as the reference. GSVA scores were calculated using the GSVA method with a Gaussian kernel, with gene set sizes restricted to 10–500 genes. Differences in GSVA scores between the MetS and control groups were assessed using limma, followed by empirical Bayes moderation. *P* values were adjusted using the Benjamini–Hochberg method, and adjusted P < 0.05 was considered significant.

2.9. Immune Cell Composition Analysis

CIBERSORTx (https://cibersortx.stanford.edu/)[37] with the LM22 signature matrix was used to estimate 22 immune cell types using 1,000 permutations. All 40 samples passed the deconvolution P < 0.05 threshold. Group differences were assessed using two-sided Wilcoxon rank-sum tests, and Spearman correlation was used for immune cell and hub-gene association analyses.

2.10. Molecular Docking

The three-dimensional structures of the hub proteins were obtained from the Protein Data Bank (PDB) in PDB format[38]. The molecular structure of clozapine was retrieved from the PubChem database and subjected to energy minimization using ChemBio3D Ultra 14.0. Protein structures were prepared using PyMOL 3.0.3 and AutoDockTools 1.5.6[39]. Crystallographic water molecules, co-crystallized ligands, and unrelated heteroatoms were removed. Polar hydrogen atoms were subsequently added, Gasteiger charges were calculated, and AutoDock atom types were assigned. The prepared receptor structures were saved in PDBQT format.

Clozapine was prepared as the ligand using AutoDockTools. The root atom and rotatable bonds were defined, after which the ligand was converted to PDBQT format. Potential binding pockets in the hub proteins were predicted using POCASA 1.1[40]. Molecular docking was then performed using AutoDock Vina 1.1.2[41]. The optimal docking conformations and protein–ligand interactions were visualized using PyMOL and Discovery Studio.

2.11. Molecular Dynamics Simulations

Molecular dynamics (MD) simulations were performed using GROMACS version 2025.2[42], based on the optimal conformations obtained from molecular docking. Each protein–ligand complex was placed in a simulation box with a minimum distance of 1.0 nm between the complex and the box boundary. The system was solvated with

simple point charge (SPC) water molecules, and Na^+ and Cl^- counterions were added to achieve electrical neutrality.

We first minimized the energy using the steepest descent algorithm, then conjugate gradient minimization. The maximum number of minimization steps was set to 10,000 for each stage. The energy-minimized systems were subsequently equilibrated under constant-volume and constant-temperature (NVT) conditions for 1 ns, followed by equilibration under constant-pressure and constant-temperature (NPT) conditions for 1 ns. Each equilibration stage consisted of 500,000 steps with a 2 fs time step.

Temperature was maintained at 300 K using the velocity-rescaling thermostat with a coupling constant of 0.1 ps. During NPT equilibration, pressure was maintained at 1 bar using isotropic Berendsen pressure coupling with a coupling constant of 2.0 ps and a compressibility of 4.5×10^{-5} bar $^{-1}$. Position restraints were applied to the protein during both equilibration stages.

Production MD simulations were conducted for 100 ns, corresponding to 50,000,000 integration steps with a time step of 2 fs. Temperature and pressure were maintained at 300 K and 1 bar, respectively, using velocity-rescaling temperature coupling and isotropic Berendsen pressure coupling. Protein and nonprotein components were coupled separately to the temperature bath.

Bonds involving hydrogen atoms were constrained using the linear constraint solver (LINCS) algorithm. A Verlet cutoff scheme was applied, with short-range electrostatic and van der Waals cutoffs both set to 1.0 nm. Long-range electrostatic interactions were calculated using the particle mesh Ewald (PME) method with fourth-order interpolation and a Fourier grid spacing of 0.16 nm. We applied three-dimensional periodic boundary conditions and included long-range dispersion corrections for energy and pressure.

We processed the resulting trajectories to correct artifacts from periodic boundary conditions, maintain the integrity of the protein–ligand complexes, and remove overall translational and rotational motions. We evaluated structural stability and conformational flexibility by calculating the root-mean-square deviation (RMSD), root-mean-square fluctuation (RMSF), radius of gyration (Rg), solvent-accessible surface area (SASA), and number of protein–ligand hydrogen bonds using the analysis modules implemented in GROMACS. Finally, molecular mechanics/Poisson–Boltzmann surface area (MM/PBSA) binding free-energy estimates were calculated using gmx_MMPBSA[43] based on the equilibrated portions of the MD trajectories after 30 ns.

3. Results

3.1. Identification of Potential Targets for Clozapine-Induced MetS

A total of 469 clozapine-related targets and 7,997 MetS-related genes were obtained from the corresponding databases. We then intersected the clozapine target-associated genes, MetS-related genes. This analysis yielded 191 overlapping genes with potential relevance to clozapine-induced MetS (Fig. 2A).

3.2. GO and KEGG Enrichment Analyses

GO enrichment analysis identified 656 BP, 84 CC, and 157 MF terms. The 10 most enriched terms meeting the FDR < 0.05 threshold are shown in Fig. 2B. The enriched BP terms were primarily related to response to xenobiotic stimulus, positive regulation of phosphatidylinositol 3-kinase/protein kinase B signal transduction and inflammatory response. In the CC category, the candidate genes were primarily enriched in the membrane raft and signaling receptor complex, whereas the enriched MF terms were predominantly associated with protein tyrosine kinase activity.

The top 20 KEGG pathway enrichment analysis at an FDR < 0.05. These included PI3K-Akt signaling pathway and Lipid and atherosclerosis (Fig. 2C). These enrichment results suggest that the candidate genes are mainly involved in kinase-mediated signaling, inflammatory responses, and lipid-related metabolic processes.

3.3. Differential Expression and Candidate Gene Identification

The GSE98895 dataset, which contains gene expression profiles of peripheral blood mononuclear cells from 20 individuals with MetS and 20 healthy controls, was then analyzed. Using an adjusted *p* value < 0.05 and |log2FC| ≥ 0.5 as the screening criteria, 809 DEGs were identified, including 393 upregulated and 416 downregulated genes (Fig. 2D). By integrating the clozapine-Met intersection targets and DEGs from the GSE98895 dataset, 13 candidate genes were obtained to identify hub genes, including *C5AR1, CCNE1, CPT1A, FPR1, GBA2, GPR35, JAK1, JAK2, LCK, MTAP, PARP1, PDE4D*, and *RAD51* (Fig. 2E).

3.4. Identification of Hub Genes

The 13 candidate genes were further analyzed using four machine learning algorithms: LASSO regression, RF, SVM-RFE, and XGBoost. These analyses were used to identify hub genes for subsequent investigation.

LASSO regression identified nine genes with nonzero coefficients: *PARP1*, *FPR1*, *GPR35*, *JAK1*, *JAK2*, *MTAP*, *PDE4D*, *RAD51*, and *C5AR1* (Fig. 3A and B). RF analysis selected *LCK*, *MTAP*, *JAK1*, *GBA2*, *PARP1*, and *PDE4D* as the six most important features according to their MeanDecreaseGini values (Fig. 3C). In the SVM-RFE analysis, the highest cross-validation accuracy, 1.00, was achieved with an eight-gene model comprising *JAK1*, *RAD51*, *C5AR1*, *JAK2*, *GPR35*, *PDE4D*, *CCNE1*, and *PARP1* (Fig. 3D). XGBoost analysis identified *JAK1*, *LCK*, *GBA2*, *MTAP*, *PARP1*, and *RAD51* as the six highest-ranked genes according to Gain values (Fig. 3E).

Thus, *PARP1* and *JAK1* were selected by all four algorithms and were designated the final hub genes for subsequent analyses (Fig. 3F). Expression analysis showed that *JAK1* expression was lower in the MetS group than in the control group, whereas *PARP1* expression was higher in the MetS group (both *p* < 0.001; Fig. 3G). A model combining *PARP1* and *JAK1* expression achieved a cross-validated area under the receiver operating characteristic curve (AUC) of 0.895, indicating discriminatory performance between individuals with MetS and healthy controls in this dataset (Fig. 3H).

3.5. GSEA of Hub Genes and GSVA Between the MetS and Control Groups

GSEA based on *JAK1* and *PARP1* expression identified several enriched BP terms, including mitotic cell cycle process, post-transcriptional regulation of gene expression, regulation of translation, mitotic cell cycle phase transition, and regulation of mitotic cell cycle phase transition (Fig. 4A).

KEGG-based GSEA also identified several enriched pathways, including fructose and mannose metabolism, amino sugar and nucleotide sugar metabolism, oxidative phosphorylation, the cell cycle, mammalian circadian rhythm,

the citrate cycle (TCA cycle), galactose metabolism, and immunodeficiency-related pathways (Fig. 4B and C). These enrichment patterns implicate cell-cycle regulation, mitochondrial energy metabolism, carbohydrate metabolism, and circadian regulation in the molecular features associated with MetS.

GSVA further identified differences in scores for several Hallmark gene sets between the MetS and control groups, including Hedgehog signaling, protein secretion, early estrogen response, interleukin-6 (IL-6)–JAK–STAT3 signaling, transforming growth factor beta (TGF-β) signaling, pancreatic β-cell signaling, and the inflammatory response (Fig. 4D). These differences in gene set scores suggest broad alterations associated with endocrine regulation, cellular signaling, protein secretion, and inflammatory processes in MetS.

3.6. Immune Cell Composition Analysis and Its Associations with JAK1 and PARP1

CIBERSORTx was used to estimate the relative proportions of 22 immune cell types in peripheral blood mononuclear cell samples. Compared with the control group, the MetS group had higher estimated proportions of resting natural killer (NK) cells and CD8 + T cells and a lower estimated proportion of resting memory CD4 + T cells (Fig. 5A). Spearman correlation analysis identified multiple associations among the estimated immune cell proportions, suggesting coordinated variation in peripheral immune cell composition (Fig. 5B). Associations between the expression levels of the two hub genes and estimated immune cell proportions were subsequently examined (Fig. 5C). *JAK1* expression was positively correlated with the estimated proportion of resting memory CD4 + T cells (Spearman's $\rho = 0.564$, $p = 1.5 \times 10^{-4}$), whereas *PARP1* expression was negatively correlated with the same immune cell population ($\rho = -0.424$, $p = 0.00639$; Fig. 5D and E). Collectively, these results indicate differences in estimated peripheral T-cell and NK-cell composition between the MetS and control groups. The opposing correlations of *JAK1* and *PARP1* expression with resting memory CD4 + T cells further indicate distinct associations between these genes and estimated peripheral immune cell composition in MetS.

3.7. Molecular Docking

We next performed molecular docking to evaluate predicted interactions between clozapine and the two hub proteins, JAK1 (PDB ID: 6DBN) and PARP1 (PDB ID: 7ONR). Clozapine yielded AutoDock Vina predicted binding affinities of − 10.0 kcal·mol^{-1} for JAK1 and − 9.5 kcal·mol^{-1} for PARP1 (Fig. 6).

In the predicted JAK1–clozapine complex, the docking pose contained several amino acid contacts and was characterized primarily by hydrophobic interactions, together with carbon–hydrogen bonding and π-related interactions. Arg1007 formed a predicted carbon–hydrogen bond with clozapine, whereas Met956 participated in a predicted π–sulfur interaction.

In the predicted PARP1–clozapine complex, the interacting residues included His862, Ser864, Tyr896, and Tyr907. Ser864 formed a predicted carbon–hydrogen bond with clozapine, whereas His862, Tyr896, and Tyr907 contributed predicted π–π stacking, π–alkyl, and other hydrophobic interactions.

Collectively, these docking results indicate computationally favorable poses for clozapine within the modeled JAK1 and PARP1 binding sites and support further investigation of these potential interactions.

3.8. Molecular Dynamics Simulations and MM/PBSA Analysis

Subsequently, we performed 100 ns MD simulations to further assess the conformational behavior of the JAK1–clozapine and PARP1–clozapine complexes. The RMSD profiles indicated that both complexes reached relatively stable conformational regimes during the simulations. The JAK1–clozapine complex underwent an initial period of conformational adjustment, with its RMSD becoming relatively stable after approximately 40 ns (Fig. 7A). In contrast, the RMSD of the PARP1–clozapine complex stabilized earlier, after approximately 20 ns (Fig. 7B). Neither complex exhibited sustained structural drift during the later portions of the trajectories, which was consistent with the persistence of the modeled complexes over the simulation period.

RMSF analysis was used to evaluate residue-level flexibility. Most residues in both JAK1 and PARP1 exhibited relatively low fluctuation values, indicating limited local conformational flexibility following clozapine binding (Fig. 7C and D). Higher fluctuations were confined to a small number of regions, indicating localized conformational flexibility.

The SASA of the JAK1–clozapine complex fluctuated within a relatively narrow range throughout the simulation, indicating generally stable protein surface exposure (Fig. 7E). Similarly, the SASA profile of the PARP1–clozapine complex showed relatively minor fluctuations, without substantial structural expansion or collapse (Fig. 7F). The Rg values of both complexes also remained relatively stable throughout the 100-ns simulations, indicating maintenance of their overall structural compactness (Fig. 7G and H).

Hydrogen-bond analysis showed that clozapine formed intermittent hydrogen bonds with both JAK1 and PARP1 during the simulations (Fig. 7 and J). Although the number of hydrogen bonds varied over time, these contacts recurred during the trajectories. Collectively, the MD results indicate conformational stability of the modeled JAK1–clozapine and PARP1–clozapine complexes during the simulated period and are consistent with the docking results.

MM/PBSA analysis yielded negative energy estimates for both complexes (Table 1). The MM/PBSA energy estimate for the JAK1–clozapine complex was − 92.749 ± 22.808 kJ·mol^{-1}. After inclusion of the interaction-entropy contribution, the entropy-corrected binding free-energy estimate was − 41.042 kJ·mol^{-1}. The PARP1–clozapine complex yielded an MM/PBSA energy estimate of − 258.029 ± 12.104 kJ·mol^{-1} and an entropy-corrected binding free-energy estimate of − 234.750 kJ·mol^{-1}.

Table 1
MM/PBSA energy components and entropy-corrected binding free-energy estimates for the JAK1–clozapine and PARP1–clozapine complexes.

Complex	ΔE_vdW (kJ·mol⁻¹)	ΔE_ele (kJ·mol⁻¹)	ΔG_PB (kJ·mol⁻¹)	ΔG_SA (kJ·mol⁻¹)	ΔG_MM/PBSA (kJ·mol⁻¹)	−TΔS_IE (kJ·mol⁻¹)	ΔG_bind,IE (kJ·mol⁻¹)
JAK1–clozapine	−190.955 ± 10.190	−56.352 ± 34.559	174.865 ± 29.473	−20.306 ± 0.524	−92.749 ± 22.808	51.706	−41.042
PARP1–clozapine	−233.081 ± 9.451	−191.830 ± 17.540	187.447 ± 23.321	−20.566 ± 0.424	−258.029 ± 12.104	23.28	−234.750

Abbreviations: ΔE_vdW, van der Waals interaction energy; ΔE_ele, electrostatic interaction energy; ΔG_PB, polar solvation energy; ΔG_SA, nonpolar solvation energy; ΔG_MM/PBSA, MM/PBSA binding energy estimate without entropy correction; −TΔS_IE, interaction entropy contribution; ΔG_bind,IE, entropy-corrected binding free-energy estimate. Energy values are reported in kJ·mol⁻¹.

4. Discussion

Metabolic syndrome has attracted increasing clinical attention because it substantially affects the quality of life and life expectancy of individuals with psychiatric disorders. Clozapine is one of the most effective antipsychotic agents and is widely regarded as the treatment of choice for treatment-resistant schizophrenia[44]. However, clozapine treatment is associated with a particularly high prevalence of MetS compared with other antipsychotic treatments[45]. Individuals receiving clozapine also have an increased risk of metabolic complications and CVD, including hypertension, diabetes mellitus, and dyslipidemia[46]. These metabolic and cardiovascular adverse effects represent a major barrier to the broader clinical use of clozapine. Thus, a more comprehensive understanding of the underlying pathological mechanisms and potential molecular targets is important for improving the prediction, prevention, and management of clozapine-associated MetS.

In the present study, 191 overlapping genes with potential relevance to clozapine-induced MetS were identified. GO and KEGG enrichment analyses indicated that these genes were primarily PI3K-Akt signaling pathway and Lipid and atherosclerosis. Previous studies have shown that clozapine can interfere with PI3K/Akt signaling, resulting in reduced Akt activation and impaired glucose uptake, which may contribute to disturbances in glucose homeostasis and insulin signaling[47,48]. Consistent with this, clozapine exposure has also been associated with increased intracellular lipid accumulation and altered lipogenic activity, accompanied by reduced Akt phosphorylation in hepatic cells[49]. These findings suggest that impaired Akt signaling may represent one of the mechanisms linking clozapine exposure to abnormalities in both glucose and lipid metabolism. In parallel, dysregulated lipid handling may further contribute to metabolic and cardiovascular complications. Experimental evidence has shown that clozapine increases oxidized low-density lipoprotein accumulation in macrophages through activation of the NOX-ROS-PPARγ-CD36 signaling axis, thereby promoting macrophage foam-cell formation, a key process involved in atherogenesis[50]. Such changes in cholesterol handling and lipid accumulation are also consistent with the dyslipidemic phenotype commonly observed in clozapine-associated metabolic disturbances. Based on these findings, we speculate that disruption of PI3K-Akt signaling and abnormal lipid metabolism may act in parallel or interact with each other, contributing to insulin resistance, lipid accumulation, and persistent metabolic dysfunction in clozapine-induced MetS. However, the specific molecular links between these pathways remain to be further clarified.

To identify key genes potentially relevant to clozapine-induced MetS, we applied four machine learning algorithms: LASSO regression, RF, SVM-RFE, and XGBoost. *JAK1* and *PARP1* were consistently selected across all four algorithms. Thus, they were designated as the final hub genes for subsequent analyses. Compared with the control group, *JAK1* expression was lower in the MetS group, whereas *PARP1* expression was higher.

We then performed GSEA and GSVA to further characterize the biological processes and signaling pathways associated with these hub genes. GSEA suggested that differences associated with *JAK1* expression involved cell-cycle regulation, translational control, mitochondrial oxidative metabolism, and carbohydrate metabolism. Enrichment patterns associated with *PARP1* expression involved glucose metabolism, the tricarboxylic acid cycle, and circadian rhythm regulation. In addition, Hallmark GSVA identified broad differences in gene set scores related to endocrine regulation, protein secretion, inflammatory signaling, and tissue homeostasis between the MetS and control groups. Together, these findings suggest that *JAK1* and *PARP1* expression may be associated with coordinated differences in immune signaling, energy metabolism, and cellular homeostasis in MetS.

JAK1 is a nonreceptor tyrosine kinase that mediates signaling downstream of interferons and multiple cytokine receptors, thereby activating transcription factors such as signal transducer and activator of transcription 1

(STAT1) and signal transducer and activator of transcription 3 (STAT3) and regulating genes involved in inflammation, immunity, and metabolism[51]. Under inflammatory conditions, IFN-γ-mediated activation of the JAK1–STAT1 pathway has been shown to impair insulin signaling, lipid storage, and adipocyte differentiation[52]. However, the metabolic consequences of JAK signaling appear to be context-dependent. Reduced expression of *JAK1* and *JAK2* has been observed in the subcutaneous adipose tissue of individuals with obesity and reduced insulin sensitivity[53], whereas treatment with JAK1/2 inhibitors has been associated with weight gain and increased body mass index in patients with myeloproliferative neoplasms[54]. Accordingly, the lower *JAK1* expression observed in the MetS group in the present study may represent a secondary adaptive response, and its biological significance may extend beyond reduced JAK1-mediated inflammatory signaling.

PARP1 is a multifunctional regulatory protein with a central role in DNA damage repair. Impaired PARP1-mediated DNA repair may reduce adipocytes' capacity to respond to genomic stress, thereby promoting cellular senescence, inflammatory mediator release, and adipose tissue dysfunction[55,56]. In contrast, sustained or excessive PARP1 activation may also contribute to metabolic dysfunction by increasing nicotinamide adenine dinucleotide (NAD^+) consumption, limiting the activity of the NAD^+-dependent deacetylase sirtuin 1 (SIRT1), and impairing peroxisome proliferator-activated receptor gamma coactivator 1-alpha (PGC-1α)-mediated mitochondrial biogenesis and oxidative metabolism[57]. These processes may promote lipid accumulation, chronic inflammation, and insulin resistance[58,59]. Beyond its role in the DNA damage response, PARP1 contributes to circadian regulation by modifying circadian locomotor output cycles kaput (CLOCK) and influencing CLOCK–brain and muscle ARNT-like 1 (BMAL1)-dependent transcription. PARP1 also participates in entraining peripheral clocks to feeding time, linking nutrient availability to the temporal regulation of metabolic activity[60]. Disruption of this regulatory process may impair the temporal coordination of glucose and lipid metabolism. Consistent with this interpretation, circadian misalignment has been associated with reduced insulin sensitivity, altered fatty acid metabolism, and increased inflammatory activity in humans[61,62]. Thus, the elevated *PARP1* expression and *PARP1*-related enrichment of metabolic and circadian pathways observed in this study may reflect dysregulated coordination among DNA damage responses, cellular energy metabolism, and circadian control in MetS.

The combined *PARP1–JAK1* model also demonstrated discriminatory performance in distinguishing individuals with MetS from healthy controls within the study dataset. These findings suggest that *PARP1* and *JAK1* warrant further investigation as a potential biomarker panel for MetS. However, because the model was developed and evaluated using a single public dataset, its diagnostic utility, particularly for clozapine-induced MetS, requires validation in independent cohorts of individuals receiving clozapine.

Hallmark GSVA revealed lower scores for the IL-6–JAK–STAT3 signaling and inflammatory response gene sets in the MetS group. Although this finding may appear inconsistent with the chronic low-grade inflammatory state commonly associated with MetS, it may reflect compensatory suppression, altered circulating immune cell composition, or differences between peripheral blood and metabolically active tissues. In addition, several gene sets involved in endocrine regulation and tissue homeostasis differed between the MetS and control groups. Previous animal studies have shown that a high-fat diet can activate Sonic Hedgehog signaling in adipose tissue, contributing to impaired glucose tolerance and insulin resistance, whereas inhibiting this pathway may ameliorate metabolic abnormalities in obese mice[63]. Experimental evidence also indicates that blocking TGF-β signaling can enhance mitochondrial biogenesis in white adipose tissue and protect against obesity, diabetes, and hepatic steatosis[64]. Together, these findings suggest that altered Hedgehog, IL-6–JAK–STAT3, and TGF-β signaling may

be associated with disrupted inflammatory, endocrine, and metabolic homeostasis in MetS. However, the direction, tissue specificity, and relevance of these pathway changes to clozapine treatment require further experimental investigation.

Immune cell composition analysis further indicated that the MetS group had higher estimated proportions of CD8 + T cells and resting NK cells and a lower estimated proportion of resting memory CD4 + T cells. CD8 + T cells and NK cells may contribute to adipose tissue inflammation and insulin resistance through cytotoxic activity and IFN-γ-related immune responses[65,66]. The lower estimated proportion of resting memory CD4 + T cells may reflect differences in cell distribution or activation state under metabolic stress[67].

JAK1 expression was positively correlated with the estimated proportion of resting memory CD4 + T cells, whereas *PARP1* expression was negatively correlated with this cell population. These opposing correlations suggest that *JAK1* and *PARP1* expression may be associated with distinct patterns of peripheral T-cell composition in MetS. Given JAK1's role in cytokine signaling and PARP1's role in DNA damage responses, energy metabolism, and inflammatory regulation, these differential associations may reflect distinct relationships between immune regulation and metabolic dysfunction. Collectively, the observed differences in estimated peripheral immune cell composition and hub-gene expression provide additional evidence of an association between immune dysregulation and MetS. However, these findings do not establish causal or direct regulatory relationships and require validation using flow cytometry, functional experiments, and clinical cohorts exposed to clozapine.

In summary, this study provides a systematic computational framework for investigating molecular mechanisms that may be relevant to clozapine-induced MetS. Through the integration of bioinformatics, network pharmacology, and machine learning approaches, *JAK1* and *PARP1* were identified as consensus candidate genes, and associated biological processes, signaling pathways, and immune cell composition patterns were characterized. Molecular docking and MD simulations provided computational evidence of favorable clozapine interactions with JAK1 and PARP1 and the persistence of the modeled complexes during the simulations. These findings provide hypotheses regarding the potential involvement of both proteins in clozapine-associated metabolic dysfunction and a basis for subsequent mechanistic and translational investigation.

Nevertheless, several limitations warrant acknowledgment. First, the transcriptomic analysis was based on a relatively small cohort of 40 samples from a single public dataset, and no independent cohort was available for external validation of the JAK1–PARP1 model. The identified candidate genes and proposed mechanisms also remain to be experimentally validated. Second, network pharmacology, CIBERSORTx, molecular docking, and MD simulations are computational approaches with inherent limitations. In particular, CIBERSORTx estimates immune cell proportions rather than directly measuring them, while docking and MD simulations do not establish direct physical binding between clozapine and JAK1 or PARP1. These findings therefore require confirmation by flow cytometry, biochemical binding assays, and functional experiments. Third, GSE98895 compared individuals with MetS with healthy controls and did not specifically include individuals receiving clozapine. Thus, the observed transcriptomic, pathway, immune, and classification results cannot be considered specific to clozapine-induced MetS. Future studies should validate these findings in independent clozapine-treated cohorts, including individuals with and without MetS.

5. Conclusion

This study identified JAK1 and PARP1 as candidate hub genes linking predicted clozapine targets with MetS-associated molecular changes. In GSE98895, their expression was associated with metabolic, inflammatory, immune, and circadian pathways. Molecular docking and MD simulations further suggested interactions between clozapine and the JAK1 and PARP1. Because GSE98895 was not derived from a clozapine-exposed cohort and the predicted protein interactions have not been experimentally validated, these findings should be regarded as hypotheses that require confirmation in independent clinical cohorts and experimental models.

Declarations

COMPETING INTERESTS

The authors declare no competing interests.

FUNDING

This work was supported by grants from the National Natural Science Foundation of

China (Nos. 82171503 and 81871052) to Chuanjun Zhuo.

AUTHOR CONTRIBUTIONS

Chuanjun Zhuo conceived, designed, and supervised the entire study, and drafted

ACKNOWLEDGEMENTS

We thank the developers of the databases that were used in this work.

DATA AVAILABILITY

Data that support the findings of this study are available from the corresponding author upon reasonable request

References

1. Taylor, M. & Perera, U. NICE CG178 Psychosis and Schizophrenia in Adults: Treatment and Management - an evidence-based guideline? *Br J Psychiatry* 206, 357–359, doi:10.1192/bjp.bp.114.155945 (2015).
2. Evaluation, I. f. H. M. a. *2023 Global Burden of Disease (GBD)*, %3Chttps://vizhub.healthdata.org/gbd-results/%3E (2025).
3. Pillinger, T., D'Ambrosio, E., McCutcheon, R. & Howes, O. D. Is psychosis a multisystem disorder? A meta-review of central nervous system, immune, cardiometabolic, and endocrine alterations in first-episode psychosis and perspective on potential models. *Mol Psychiatry* 24, 776–794, doi:10.1038/s41380-018-0058-9 (2019).
4. Plana-Ripoll, O. *et al.* A comprehensive analysis of mortality-related health metrics associated with mental disorders: a nationwide, register-based cohort study. *Lancet* 394, 1827–1835, doi:10.1016/s0140-

6736(19)32316-5 (2019).

5. Manu, P. *et al.* Weight gain and obesity in schizophrenia: epidemiology, pathobiology, and management. *Acta Psychiatr Scand* 132, 97–108, doi:10.1111/acps.12445 (2015).
6. Fahed, G. *et al.* Metabolic Syndrome: Updates on Pathophysiology and Management in 2021. *International journal of molecular sciences* 23, doi:10.3390/ijms23020786 (2022).
7. Alberti, K. G. *et al.* Harmonizing the metabolic syndrome: a joint interim statement of the International Diabetes Federation Task Force on Epidemiology and Prevention; National Heart, Lung, and Blood Institute; American Heart Association; World Heart Federation; International Atherosclerosis Society; and International Association for the Study of Obesity. *Circulation* 120, 1640–1645, doi:10.1161/circulationaha.109.192644 (2009).
8. Vancampfort, D. *et al.* Risk of metabolic syndrome and its components in people with schizophrenia and related psychotic disorders, bipolar disorder and major depressive disorder: a systematic review and meta-analysis. *World Psychiatry* 14, 339–347, doi:10.1002/wps.20252 (2015).
9. Manta, A. *et al.* Metabolic syndrome in patients with schizophrenia: Underlying mechanisms and therapeutic approaches (Review). *Mol Med Rep* 31, doi:10.3892/mmr.2025.13479 (2025).
10. Burschinski, A. *et al.* Metabolic side effects in persons with schizophrenia during mid- to long-term treatment with antipsychotics: a network meta-analysis of randomized controlled trials. *World Psychiatry* 22, 116–128, doi:10.1002/wps.21036 (2023).
11. Pillinger, T. *et al.* Comparative effects of 18 antipsychotics on metabolic function in patients with schizophrenia, predictors of metabolic dysregulation, and association with psychopathology: a systematic review and network meta-analysis. *Lancet Psychiatry* 7, 64–77, doi:10.1016/s2215-0366(19)30416-x (2020).
12. Luykx, J. J., Stam, N., Tanskanen, A., Tiihonen, J. & Taipale, H. In the aftermath of clozapine discontinuation: comparative effectiveness and safety of antipsychotics in patients with schizophrenia who discontinue clozapine. *Br J Psychiatry* 217, 498–505, doi:10.1192/bjp.2019.267 (2020).
13. Carli, M. *et al.* Atypical Antipsychotics and Metabolic Syndrome: From Molecular Mechanisms to Clinical Differences. *Pharmaceuticals (Basel)* 14, doi:10.3390/ph14030238 (2021).
14. Gressier, F., Porcelli, S., Calati, R. & Serretti, A. Pharmacogenetics of clozapine response and induced weight gain: A comprehensive review and meta-analysis. *Eur Neuropsychopharmacol* 26, 163–185, doi:10.1016/j.euroneuro.2015.12.035 (2016).
15. Kim, S. *et al.* PubChem 2023 update. *Nucleic acids research* 51, D1373-d1380, doi:10.1093/nar/gkac956 (2023).
16. Keiser, M. J. *et al.* Predicting new molecular targets for known drugs. *Nature* 462, 175–181, doi:10.1038/nature08506 (2009).
17. Gallo, K., Goede, A., Preissner, R. & Gohlke, B. O. SuperPred 3.0: drug classification and target prediction-a machine learning approach. *Nucleic Acids Res* 50, W726-w731, doi:10.1093/nar/gkac297 (2022).
18. Yao, Z. J. *et al.* TargetNet: a web service for predicting potential drug-target interaction profiling via multi-target SAR models. *J Comput Aided Mol Des* 30, 413–424, doi:10.1007/s10822-016-9915-2 (2016).
19. Daina, A., Michielin, O. & Zoete, V. SwissTargetPrediction: updated data and new features for efficient prediction of protein targets of small molecules. *Nucleic acids research* 47, W357-w364, doi:10.1093/nar/gkz382 (2019).

20. Wang, X. *et al.* PharmMapper 2017 update: a web server for potential drug target identification with a comprehensive target pharmacophore database. *Nucleic Acids Res* 45, W356-w360, doi:10.1093/nar/gkx374 (2017).
21. UniProt: the Universal Protein Knowledgebase in 2023. *Nucleic Acids Res* 51, D523-d531, doi:10.1093/nar/gkac1052 (2023).
22. Stelzer, G. *et al.* The GeneCards Suite: From Gene Data Mining to Disease Genome Sequence Analyses. *Current protocols in bioinformatics* 54, 1.30.31–31.30.33, doi:10.1002/cpbi.5 (2016).
23. Amberger, J. S., Bocchini, C. A., Scott, A. F. & Hamosh, A. OMIM.org: leveraging knowledge across phenotype-gene relationships. *Nucleic Acids Res* 47, D1038-d1043, doi:10.1093/nar/gky1151 (2019).
24. Sherman, B. T. *et al.* DAVID: a web server for functional enrichment analysis and functional annotation of gene lists (2021 update). *Nucleic acids research* 50, W216-w221, doi:10.1093/nar/gkac194 (2022).
25. Clough, E. & Barrett, T. The Gene Expression Omnibus Database. *Methods Mol Biol* 1418, 93–110, doi:10.1007/978-1-4939-3578-9_5 (2016).
26. D'Amore, S. *et al.* Identification of miR-9-5p as direct regulator of ABCA1 and HDL-driven reverse cholesterol transport in circulating CD14 + cells of patients with metabolic syndrome. *Cardiovasc Res* 114, 1154–1164, doi:10.1093/cvr/cvy077 (2018).
27. Ritchie, M. E. *et al.* limma powers differential expression analyses for RNA-sequencing and microarray studies. *Nucleic Acids Res* 43, e47, doi:10.1093/nar/gkv007 (2015).
28. Friedman, J., Hastie, T. & Tibshirani, R. Regularization Paths for Generalized Linear Models via Coordinate Descent. *J Stat Softw* 33, 1–22 (2010).
29. Breiman, L. Random Forests. *Machine Learning* 45, 5–32, doi:10.1023/A:1010933404324 (2001).
30. Guyon, I., Weston, J., Barnhill, S. & Vapnik, V. Gene Selection for Cancer Classification using Support Vector Machines. *Machine Learning* 46, 389–422, doi:10.1023/A:1012487302797 (2002).
31. Kuhn, M. Building Predictive Models in R Using the caret Package. *Journal of Statistical Software* 28, 1–26, doi:10.18637/jss.v028.i05 (2008).
32. Chen, T. & Guestrin, C. in *Proceedings of the 22nd ACM SIGKDD International Conference on Knowledge Discovery and Data Mining* 785–794 (Association for Computing Machinery, San Francisco, California, USA, 2016).
33. Subramanian, A. *et al.* Gene set enrichment analysis: a knowledge-based approach for interpreting genome-wide expression profiles. *Proc Natl Acad Sci U S A* 102, 15545–15550, doi:10.1073/pnas.0506580102 (2005).
34. Liberzon, A. *et al.* The Molecular Signatures Database (MSigDB) hallmark gene set collection. *Cell Syst* 1, 417–425, doi:10.1016/j.cels.2015.12.004 (2015).
35. Wu, T. *et al.* clusterProfiler 4.0: A universal enrichment tool for interpreting omics data. *Innovation (Camb)* 2, 100141, doi:10.1016/j.xinn.2021.100141 (2021).
36. Hänzelmann, S., Castelo, R. & Guinney, J. GSVA: gene set variation analysis for microarray and RNA-seq data. *BMC Bioinformatics* 14, 7, doi:10.1186/1471-2105-14-7 (2013).
37. Newman, A. M. *et al.* Determining cell type abundance and expression from bulk tissues with digital cytometry. *Nat Biotechnol* 37, 773–782, doi:10.1038/s41587-019-0114-2 (2019).
38. Burley, S. K. *et al.* RCSB Protein Data Bank: powerful new tools for exploring 3D structures of biological macromolecules for basic and applied research and education in fundamental biology, biomedicine,

biotechnology, bioengineering and energy sciences. *Nucleic Acids Res* 49, D437-d451, doi:10.1093/nar/gkaa1038 (2021).

39. Morris, G. M. *et al.* AutoDock4 and AutoDockTools4: Automated docking with selective receptor flexibility. *J Comput Chem* 30, 2785–2791, doi:10.1002/jcc.21256 (2009).
40. Yu, J., Zhou, Y., Tanaka, I. & Yao, M. Roll: a new algorithm for the detection of protein pockets and cavities with a rolling probe sphere. *Bioinformatics* 26, 46–52, doi:10.1093/bioinformatics/btp599 (2010).
41. Eberhardt, J., Santos-Martins, D., Tillack, A. F. & Forli, S. AutoDock Vina 1.2.0: New Docking Methods, Expanded Force Field, and Python Bindings. *Journal of chemical information and modeling* 61, 3891–3898, doi:10.1021/acs.jcim.1c00203 (2021).
42. Abraham, M. J. *et al.* GROMACS: High performance molecular simulations through multi-level parallelism from laptops to supercomputers. *SoftwareX* 1–2, 19–25, doi:https://doi.org/10.1016/j.softx.2015.06.001 (2015).
43. Valdés-Tresanco, M. S., Valdés-Tresanco, M. E., Valiente, P. A. & Moreno, E. gmx_MMPBSA: A New Tool to Perform End-State Free Energy Calculations with GROMACS. *J Chem Theory Comput* 17, 6281–6291, doi:10.1021/acs.jctc.1c00645 (2021).
44. Howes, O. D. *et al.* Treatment-Resistant Schizophrenia: Treatment Response and Resistance in Psychosis (TRRIP) Working Group Consensus Guidelines on Diagnosis and Terminology. *Am J Psychiatry* 174, 216–229, doi:10.1176/appi.ajp.2016.16050503 (2017).
45. Masuda, T., Misawa, F., Takase, M., Kane, J. M. & Correll, C. U. Association With Hospitalization and All-Cause Discontinuation Among Patients With Schizophrenia on Clozapine vs Other Oral Second-Generation Antipsychotics: A Systematic Review and Meta-analysis of Cohort Studies. *JAMA Psychiatry* 76, 1052–1062, doi:10.1001/jamapsychiatry.2019.1702 (2019).
46. Quek, Y. F. *et al.* Metabolic syndrome and cardiovascular risk between clozapine and non-clozapine antipsychotic users with schizophrenia. *Asian J Psychiatr* 74, 103192, doi:10.1016/j.ajp.2022.103192 (2022).
47. Fehsel, K. *et al.* Neuroreceptor Inhibition by Clozapine Triggers Mitohormesis and Metabolic Reprogramming in Human Blood Cells. *Cells* 13, doi:10.3390/cells13090762 (2024).
48. Fehsel, K. Metabolic Side Effects from Antipsychotic Treatment with Clozapine Linked to Aryl Hydrocarbon Receptor (AhR) Activation. *Biomedicines* 12, doi:10.3390/biomedicines12102294 (2024).
49. Tsai, I. L., Lin, S. C., Lin, L., Tsai, P. S. & Chen, S. Y. Adiponectin improves clozapine-induced lipid accumulation and inflammation without affecting insulin resistance. *Open life sciences* 21, 20251333, doi:10.1515/biol-2025-1333 (2026).
50. Chen, C. H. *et al.* Atypical antipsychotic drugs deregulate the cholesterol metabolism of macrophage-foam cells by activating NOX-ROS-PPARγ-CD36 signaling pathway. *Metabolism: clinical and experimental* 123, 154847, doi:10.1016/j.metabol.2021.154847 (2021).
51. Spinelli, F. R., Colbert, R. A. & Gadina, M. JAK1: Number one in the family; number one in inflammation? *Rheumatology (Oxford)* 60, ii3-ii10, doi:10.1093/rheumatology/keab024 (2021).
52. McGillicuddy, F. C. *et al.* Interferon gamma attenuates insulin signaling, lipid storage, and differentiation in human adipocytes via activation of the JAK/STAT pathway. *J Biol Chem* 284, 31936–31944, doi:10.1074/jbc.M109.061655 (2009).
53. Strączkowski, M. *et al.* The effect of moderate weight loss, with or without (1, 3)(1, 6)-β-glucan addition, on subcutaneous adipose tissue inflammatory gene expression in young subjects with uncomplicated obesity.

Endocrine 61, 275–284, doi:10.1007/s12020-018-1619-z (2018).

54. Sapre, M. *et al.* Metabolic Effects of JAK1/2 Inhibition in Patients with Myeloproliferative Neoplasms. *Sci Rep* 9, 16609, doi:10.1038/s41598-019-53056-x (2019).
55. Lee, G. *et al.* SREBP1c-PARP1 axis tunes anti-senescence activity of adipocytes and ameliorates metabolic imbalance in obesity. *Cell Metab* 34, 702–718.e705, doi:10.1016/j.cmet.2022.03.010 (2022).
56. Gustafson, B., Nerstedt, A., Spinelli, R., Beguinot, F. & Smith, U. Type 2 Diabetes, Independent of Obesity and Age, Is Characterized by Senescent and Dysfunctional Mature Human Adipose Cells. *Diabetes* 71, 2372–2383, doi:10.2337/db22-0003 (2022).
57. Bai, P. *et al.* PARP-1 inhibition increases mitochondrial metabolism through SIRT1 activation. *Cell Metab* 13, 461–468, doi:10.1016/j.cmet.2011.03.004 (2011).
58. Mukhopadhyay, P. *et al.* PARP inhibition protects against alcoholic and non-alcoholic steatohepatitis. *J Hepatol* 66, 589–600, doi:10.1016/j.jhep.2016.10.023 (2017).
59. Rappou, E. *et al.* Weight Loss Is Associated With Increased NAD(+)/SIRT1 Expression But Reduced PARP Activity in White Adipose Tissue. *J Clin Endocrinol Metab* 101, 1263–1273, doi:10.1210/jc.2015-3054 (2016).
60. Asher, G. *et al.* Poly(ADP-ribose) polymerase 1 participates in the phase entrainment of circadian clocks to feeding. *Cell* 142, 943–953, doi:10.1016/j.cell.2010.08.016 (2010).
61. Leproult, R., Holmbäck, U. & Van Cauter, E. Circadian misalignment augments markers of insulin resistance and inflammation, independently of sleep loss. *Diabetes* 63, 1860–1869, doi:10.2337/db13-1546 (2014).
62. Wefers, J. *et al.* Circadian misalignment induces fatty acid metabolism gene profiles and compromises insulin sensitivity in human skeletal muscle. *Proc Natl Acad Sci U S A* 115, 7789–7794, doi:10.1073/pnas.1722295115 (2018).
63. Yao, Q., Liu, J., Xiao, L. & Wang, N. Sonic hedgehog signaling instigates high-fat diet-induced insulin resistance by targeting PPARγ stability. *J Biol Chem* 294, 3284–3293, doi:10.1074/jbc.RA118.004411 (2019).
64. Yadav, H. *et al.* Protection from obesity and diabetes by blockade of TGF-β/Smad3 signaling. *Cell Metab* 14, 67–79, doi:10.1016/j.cmet.2011.04.013 (2011).
65. Nishimura, S. *et al.* CD8 + effector T cells contribute to macrophage recruitment and adipose tissue inflammation in obesity. *Nat Med* 15, 914–920, doi:10.1038/nm.1964 (2009).
66. Wouters, K. *et al.* NK cells in human visceral adipose tissue contribute to obesity-associated insulin resistance through low-grade inflammation. *Clin Transl Med* 10, e192, doi:10.1002/ctm2.192 (2020).
67. Mauro, C. *et al.* Obesity-Induced Metabolic Stress Leads to Biased Effector Memory CD4(+) T Cell Differentiation via PI3K p110δ-Akt-Mediated Signals. *Cell Metab* 25, 593–609, doi:10.1016/j.cmet.2017.01.008 (2017).

Figures

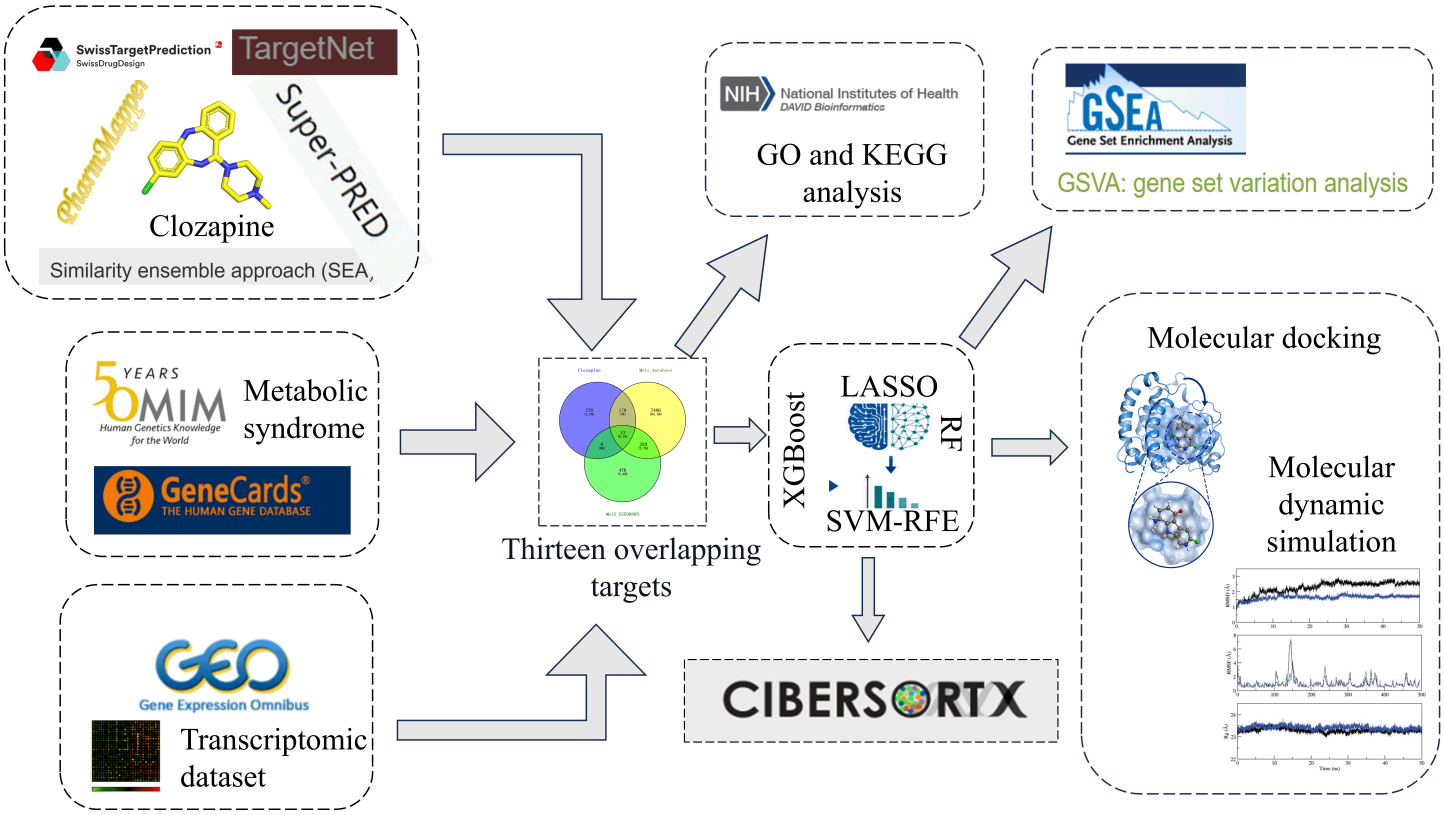


Figure 1

Overall workflow for identifying potential molecular targets and mechanisms linking clozapine to MetS.

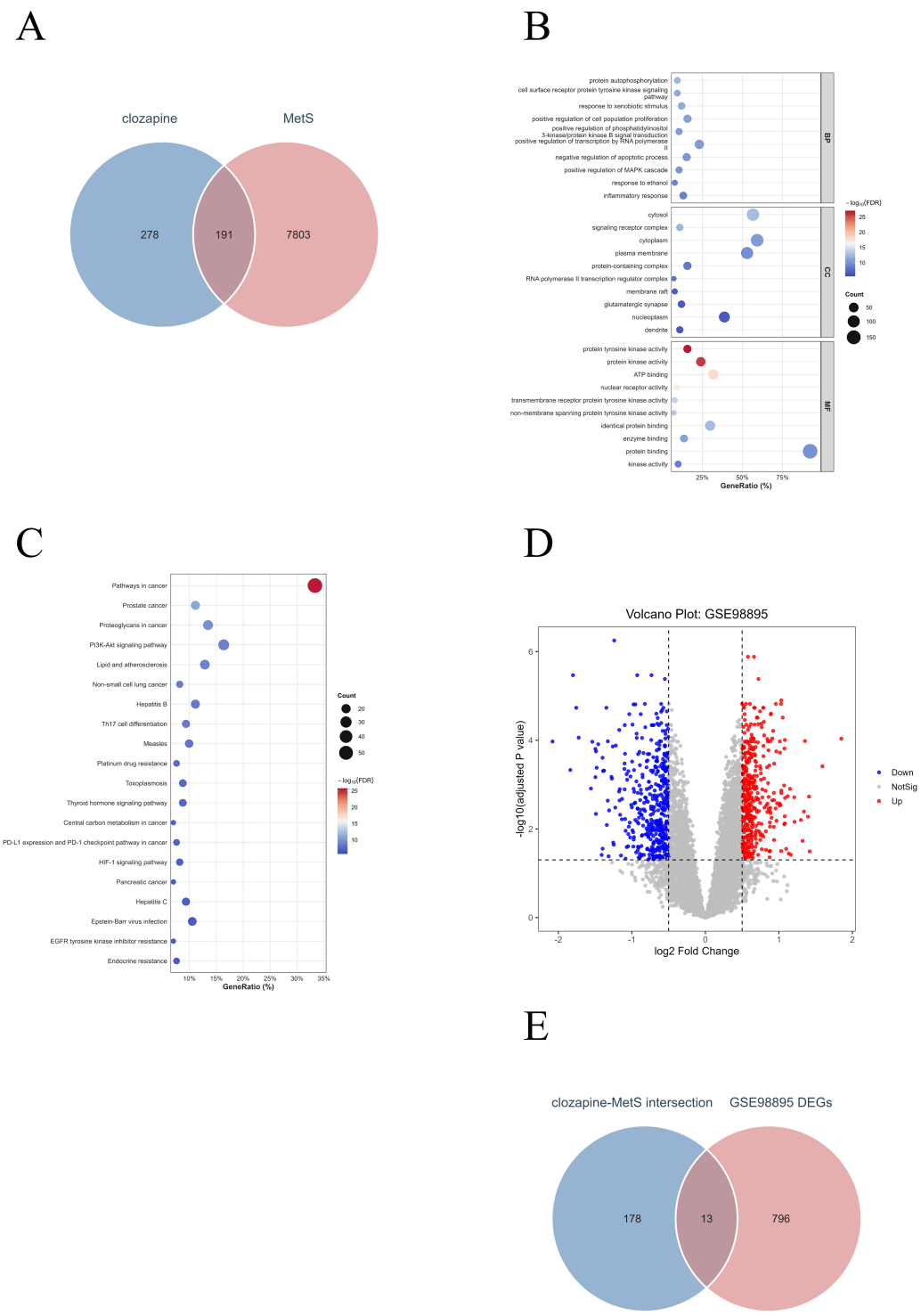


Figure 2

Identification and functional characterization of candidate genes associated with clozapine and MetS. (A) Venn diagram showing the overlap between predicted clozapine-related targets and MetS-related genes; (B) Gene Ontology (GO) enrichment analysis of the overlapping genes, including biological process (BP), cellular component (CC), and molecular function (MF) categories; (C) Kyoto Encyclopedia of Genes and Genomes (KEGG) pathway enrichment analysis of the overlapping genes; (D) volcano plot of differentially expressed genes (DEGs)

between the MetS and control groups; (E) venn diagram showing the intersection between clozapine–MetS overlapping genes and DEGs.

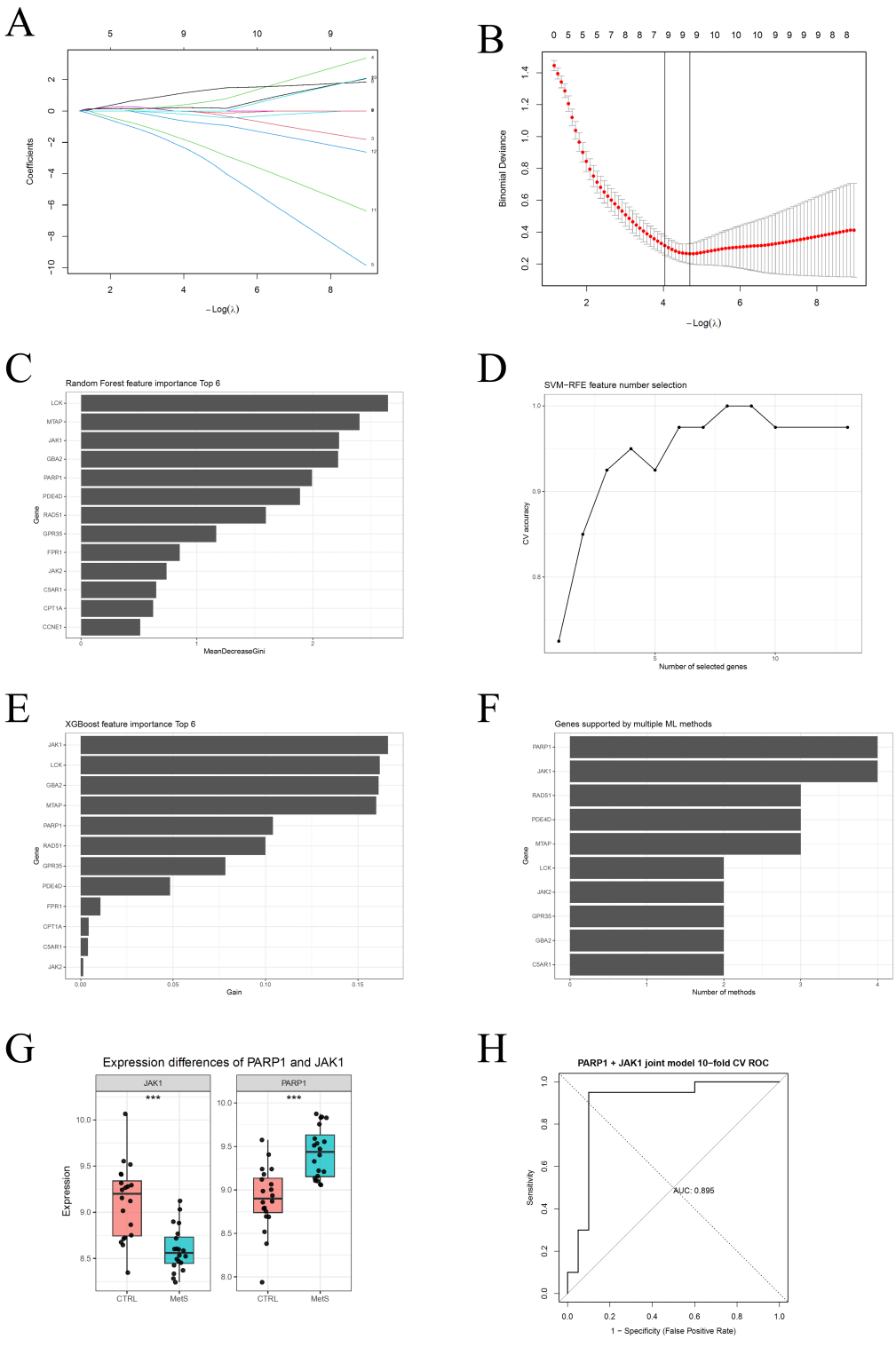


Figure 3

Machine-learning identification and evaluation of the discriminatory performance of candidate genes.(A) LASSO coefficient profiles of the candidate genes; (B) ten-fold cross-validation curve for for selection of the optimal LASSO regularization parameter; (C) RF feature importance based on MeanDecreaseGini; (D) cross-validation

accuracy for different numbers of features in SVM-RFE; (E) XGBoost feature importance based on Gain; (F) candidate genes selected by multiple machine learning algorithms; (G) expression levels of *JAK1* and *PARP1*in the control and MetS groups. Differences were assessed using two-sided Wilcoxon rank-sum tests, with Benjamini–Hochberg adjustment across the two genes; ***adjusted $p < 0.001$; (H) ten-fold cross-validated receiver operating characteristic (ROC) curve for the combined *JAK1–PARP1*logistic regression model.

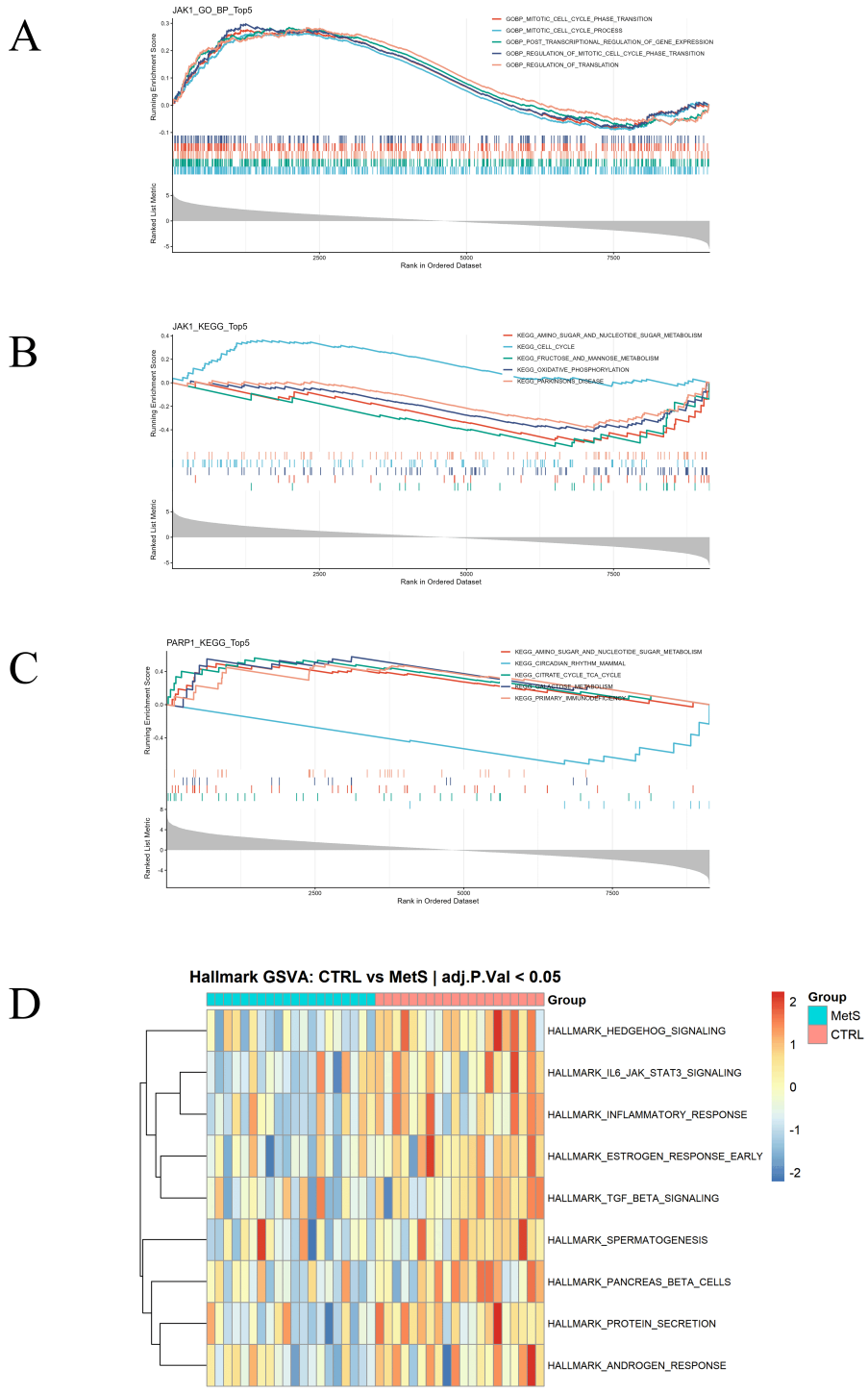


Figure 4

Functional pathway analyses associated with *JAK1*and *PARP1* expression.(A) GSEA of GO BPs associated with *JAK1*expression; (B) GSEA of KEGG pathways associated with *JAK1* expression; (C) GSEA of KEGG pathways associated with *PARP1* expression; (D) GSVA heatmap showing Hallmark gene sets that differed between the control and MetS groups.

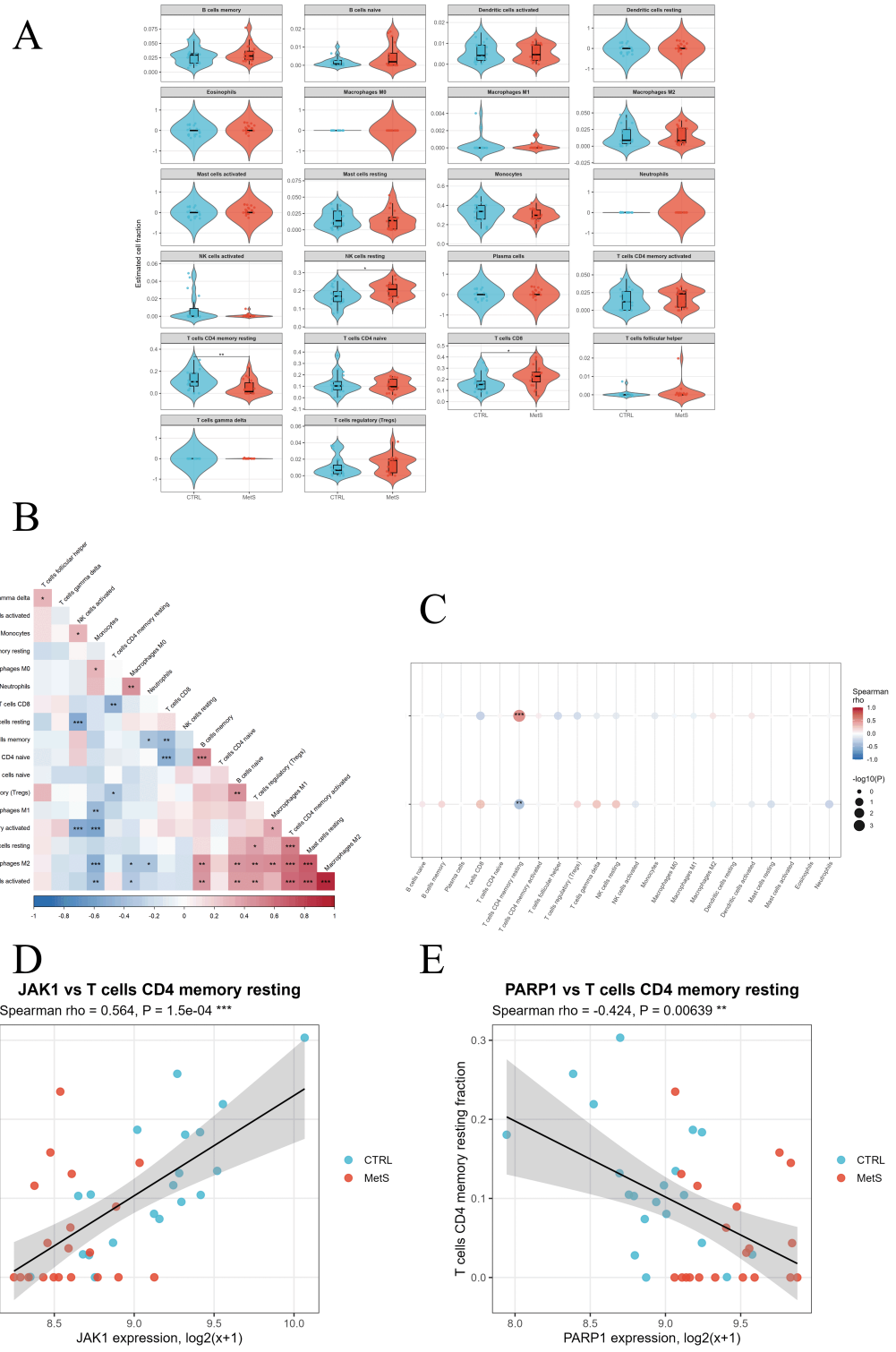


Figure 5

Estimated immune cell composition and its associations with *JAK1* and *PARP1*expression. (A) Comparison of the estimated proportions of 22 immune cell types between the control and MetS groups. Differences were assessed using two-sided Wilcoxon rank-sum tests; (B) spearman correlation matrix of the estimated immune cell proportions; (C) spearman correlations between *JAK1* and *PARP1* expression and the estimated proportions of 22 immune cell types; (D) association between *JAK1*expression and the estimated proportion of resting memory CD4+ T cells; (E) association between *PARP1* expression and the estimated proportion of resting memory CD4+ T cells. Significance annotations are based on unadjusted two-sided *P* values: *P* < 0.05, **P* < 0.01, and ***P*< 0.001.

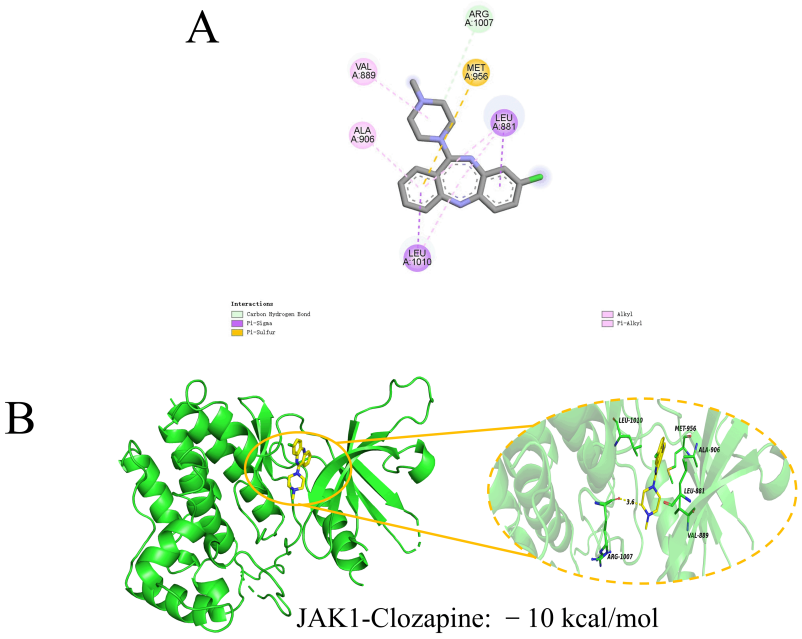


Figure 6

Molecular docking of clozapine with JAK1 and PARP1. (A) Two-dimensional interaction map of clozapine within the predicted JAK1 binding pocket; (B) three-dimensional representation of the predicted JAK1–clozapine docking pose; (C) two-dimensional interaction map of clozapine within the predicted PARP1 binding pocket; (D) three-dimensional representation of the predicted PARP1–clozapine docking pose.

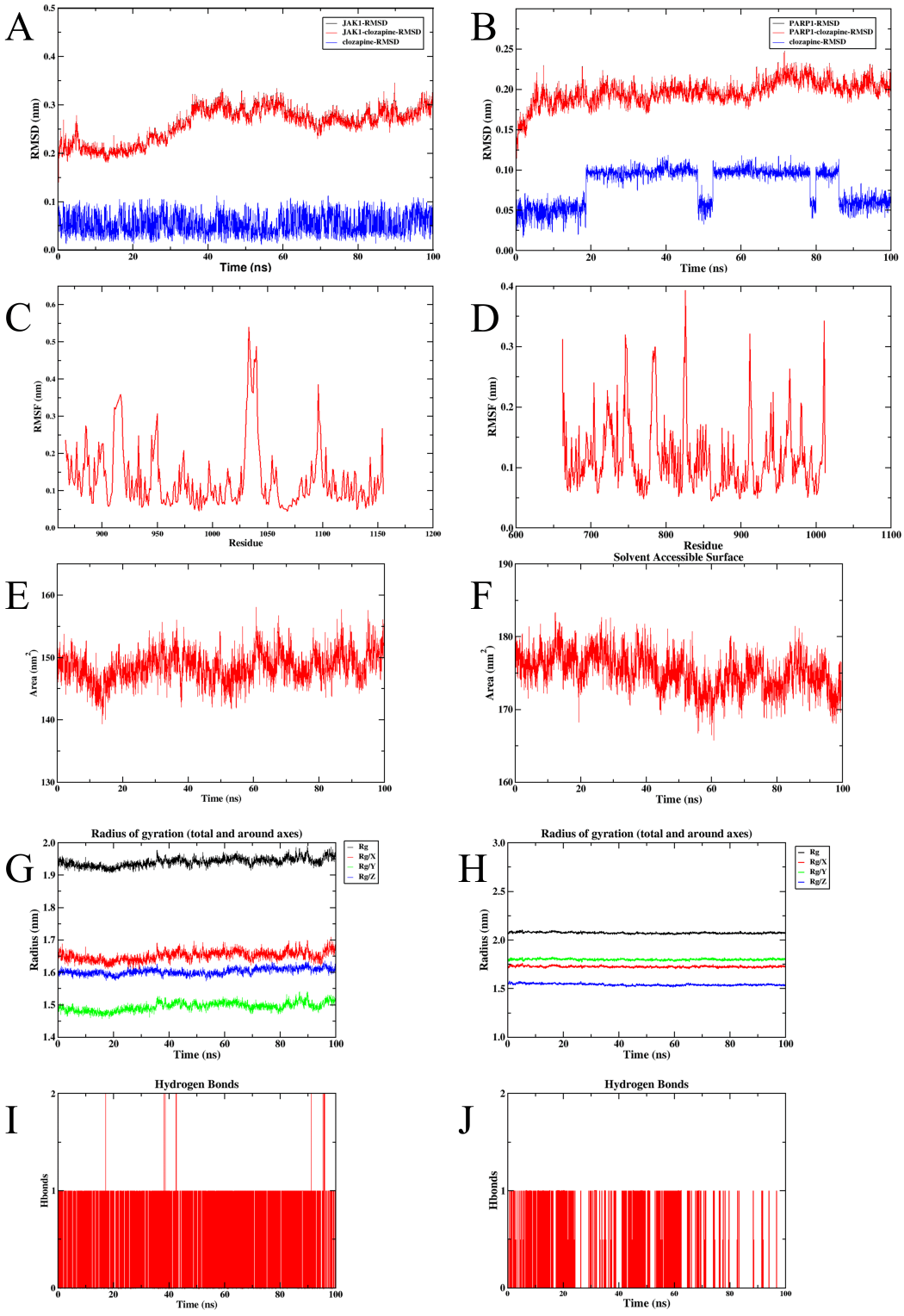


Figure 7

Molecular dynamics simulations of the JAK1–clozapine and PARP1–clozapine complexes. (A) RMSD profiles of JAK1, the JAK1–clozapine complex, and clozapine; (B) RMSD profiles of PARP1, the PARP1–clozapine complex, and clozapine; (C) residue-level RMSF profile of JAK1; (D) residue-level RMSF profile of PARP1; (E) solvent-accessible surface area (SASA) of JAK1; (F) SASA of PARP1; (G) radius of gyration (Rg) of the JAK1 backbone; (H) Rg of the PARP1 backbone; (I) number of protein–ligand hydrogen bonds between JAK1 and clozapine; (J) number of protein–ligand hydrogen bonds between PARP1 and clozapine.